Formation and Annealing Behavior of Nanocrystalline Ferrite in Fe-0.89C Spheroidite Steel Produced by Ball Milling

Y. XU, Z.G. LIU, M. UMEMOTO, and K. TSUCHIYA

Nanocrystalline ferrite formation by ball milling in Fe-0.89C spheroidite steel and its annealing behavior have been studied through microstructure observations and microhardness measurements. It was found that at the early stage of ball milling, the dislocation density increases and dislocation cells form due to plastic deformation. At the middle stage of ball milling, a layered nanocrystalline structure forms near the surface of the powder by localized severe deformation. The microhardness of nanocrystalline ferrite (10 GPa) is much higher than that of work-hardened ferrite (4 GPa). Together with the nanocrystallization of ferrite, the dissolution of cementite was observed. At the final stage of ball milling, equiaxed nanocrystalline ferrite forms from layered nanocrystalline ferrite by increasing the local misorientation. By annealing the milled powders, recrystallization was observed in the work-hardened ferrite region, while in the nanocrystalline ferrite region, a slow grain growth was observed instead of recrystallization.

1. INTRODUCTION

NANOCRYSTALLINE materials have attracted considerable scientific interest in the last few decades because of their unusual properties, which are normally attributed to an ultrafine grain size in the nanometer range and a large volume fraction of grain boundaries.[1,2] Various methods have been developed to obtain nanocrystalline materials, such as ball milling,[3,4,5] crystallization from an amorphous state,[6,7] equal-channel angular pressing,[8,9] torsion straining under high pressure,[10,11] *etc.* Among these, ball milling is the simplest method and can effectively refine the grains down to the nanometer scale for most metals, alloys, and intermetallics.[3–5,12–14] Therefore, ball milling has been widely used to produce nanocrystalline materials. The general understanding of the nanocrystallization mechanism is that ball milling results in the deformation of milled powders, leading to gradual grain refinement, and results in the final nanocrystalline structure. Fecht *et al.*[15] proposed that shear bands might be a precursor for nanocrystalline structure formation by studying the ball milling of an AlRu compound. Huang *et al.*[16] also found the existence of shear bands and a number of twins in a study on ball-milled Cu powders. The formation of subgrain was suggested to take place either in the shear bands, at the tip of them, at the tip of the twin boundaries, or at the edge of the larger grains. Therefore, it is expected that the shear band is a necessary precursor for nanocrystalline formation. However, in recent study on cryomilling Zn powder, the formation of a large number of small grains (2 to 6 nm) in the very early cryomilling stage was explained by a dynamic recrystallization mechanism.[17]

Y. XU, Associate Professor, is with the Institute of Metal Research, Chinese Academy of Sciences, Shenyang 110015, P.R. China. Contact e-mail: yanxu630@hotmail.com Z.G. LIU, formerly Assistant Professor, Department of Production Systems Engineering, Toyohashi University of Technology, is Guest Scientist, Materials Division, Faculty of Engineering, Ulm University, D-89081 Ulm, Germany. M. UMEMOTO, Professor, and K. TSUCHIYA, Associate Professor, are with the Department of Production Systems Engineering, Toyohashi University of Technology, Toyohashi 441-8580, Japan.

Manuscript submitted October 19, 2001.

Although the direct microstructural observations by transmission electron microscopy (TEM) were carried out for the powders that had completed nanocrystallization, the structural change during ball milling was usually estimated by indirect methods such as grain-size estimation by X-ray diffraction line broadening. The description of the nanocrystallization process is less convincing due to the absence of direct microstructural observations. Therefore, the clear and detailed process of microstructural evolution during nanocrystallization has not been well understood.

As the most widely used material, steel has been well studied to improve its mechanical properties by the refinement of microstructure. The nanocrystallization of steel is expected to improve its properties further. The formation of nanocrystalline ferrite in Fe-C alloys (including pure iron) by ball milling has been investigated.[3,18–26] The process of microstructure evolution during pure iron nanocrystallization has been studied by conventional horizontal low-energy ball milling, and a layered-structure nanocrystalline ferrite was observed.[21] It has been reported[25,26] that, during ball milling of Fe-C alloys with a (ferrite + cementite) two-phase structure, ferrite grains are refined to 10 nm and cementite dissolves into ferrite grain boundaries to form an amorphous layer with a high carbon concentration. The cementite dissolution was also observed in heavily drawn pearlite steel wires,[27,28,29] and there exist different explanations about the mechanism of cementite dissolution during severe plastic deformation.[25–29]

The thermal stability of a nanocrystal is another important issue. Several research studies on the thermal stability of nanocrystalline ferrite (pure Fe) have been carried out recently.[21,30,31] It was found that the grain growth rate of nanocrystalline ferrite is much lower than that of coarse-grained ferrite. The difference in the grain growth rate between nanocrystalline ferrite and conventional coarse-grained ferrite was considered to be due to either the lowered atomic-jump frequency or higher activation energy in nanocrystalline ferrite.[30] The pinning effect on the grain boundary was also used to explain the slow grain growth of nanocrystalline materials.[31,32] However, a large number of factors controlling grain growth and their complex interactions make the understanding of grain growth in nanocrystalline materials very difficult.

In the present study, the formation process of a nanocrystalline structure by low-energy ball milling was investigated in an Fe-0.89C spheroidite steel using scanning electron microscopy (SEM) and TEM. Special attention was paid to the intermediate stage of nanostructure formation by studying specimens containing both nanocrystalline ferrite and work-hardened ferrite. The influence of cementite on the formation of nanocrystalline ferrite, as well as the dissolution of cementite into ferrite, was discussed. The thermal stability of nanocrystalline ferrite was studied by annealing the ball-milled powders. Comparison was made on the grain-growth behavior of the work-hardened ferrite and nanocrystalline ferrite.

II. EXPERIMENTAL PROCEDURES

The material used in the present study was an Fe-0.89C spheroidite steel (0.887C, 0.25Si, 0.50Mn, 0.005P, 0.0044S, 0.036Al, 0.0048N, 0.003Ni, 0.30Cr, and 0.003Ti, in mass pct). The chips, with a thickness of less than 1 mm and a length of several millimeters, were cut from alloy blocks, loaded into a stainless steel pot with steel balls (SUJ2), and ball-milled under a pure Ar atmosphere using a conventional horizontal low-energy ball mill. The weight ratio of the ball-to-powder mixture was 100:1, and the milling time was up to 1800 ks. Part of the milled powders was sealed in quartz tubes with a pure Ar protective atmosphere and annealed at different temperatures for 3.6 ks. The as-milled and annealed powders were subjected to structural observations by SEM (JEOL* JSM-6300) after etching with 3 pct Nital. The TEM observations were carried out on an Hitachi H-800 microscope working at 200 kV. High-resolution electron microscopy (HREM) observations were performed on a JEOL JEM-2010 working at 200 kV. Microhardness measurements were carried out using a MVK-G1 Vickers hardness tester. Dynamic microhardness was performed using a DUH-W201S dynamic ultramicrohardness tester.

*JEOL is a trademark of Japan Electron Optics Ltd., Tokyo.

III. EXPERIMENTAL RESULTS

A. *Microstructural and Microhardness Evolution Along Ball-Milling Time*

1. *The SEM observation results*

The microstructural evolution by ball milling has been studied by SEM observations. Figure 1 shows the microstructural evolution of ball-milled powder with milling time. The starting materials have a uniform microstructure of ferrite and spherical cementite particles. In the powders milled for 36 ks (Figure 1(a)), a band structure with a thickness of 0.1 to 0.3 μm is observed near the surface region of the powders. A conventional work-hardened structure with cementite particles and deformed ferrite grains is seen in the interior of the powders. With increasing milling time to 360 ks (Figure 1(b)), the band structure on the surface evolves into a uniform structure (labeled “nano” in the picture), that is, Nital etching could not reveal the structural detail by SEM observation. The spherical cementite particles are hard to observe in this region. This region was found to be nanostructured ferrite by TEM observation, as will be mentioned in the next section. The band structure is sometimes seen in between the nano and work-hardened regions, as is shown here. Therefore, the band structure is regarded as the intermediate stage of nanocrystalline ferrite formation. The band structure shown in Figures 1(a) or (b) is considered to be locally heavily deformed regions. Although the nature of the band structure is not clear, it may be a kind of deformation band such as a microband or shear band. Longer milling time to 1800 ks leads to the powder refinement and formation of a uniform nanocrystalline structure in the entire area of

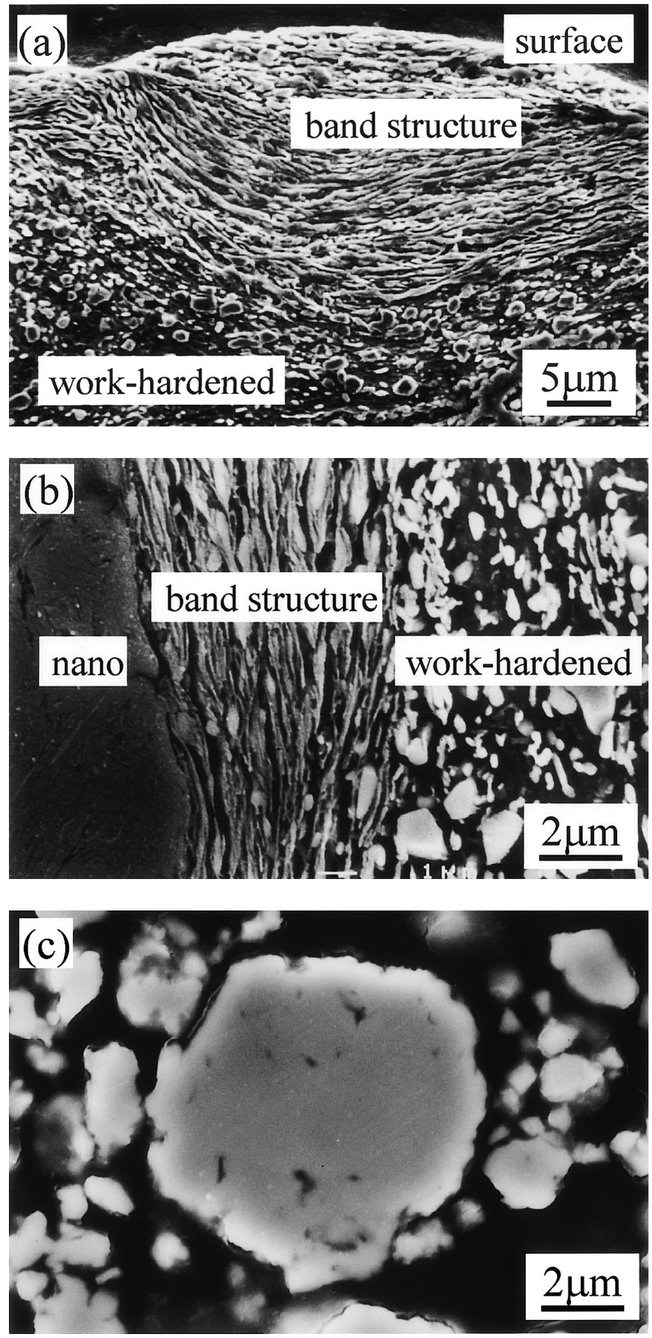

Fig. 1—Microstructure evolution with ball milling for (*a*) 36 ks, (*b*) 360 ks, and (*c*) 1800 ks.

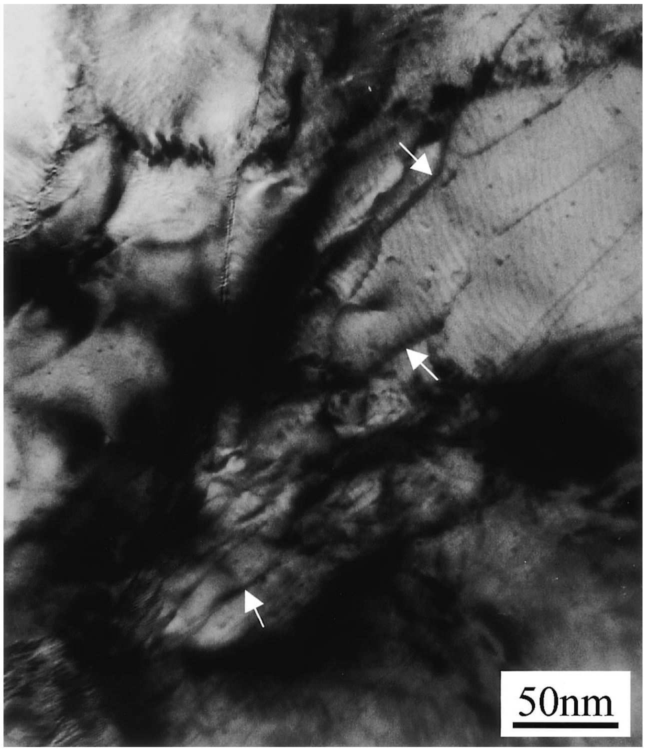

Fig. 2—Typical TEM images of the interior region in the powder milled for 360 ks.

all the powders, although the powder size is not uniform (Figure 1(c)). It is noted that cementite particles appear to dissolve into nanocrystalline ferrite completely.

2. *The TEM and HREM observation results*

Figure 2 shows the TEM image in the interior region of the Fe-0.89C spheroidite powders milled for 360 ks. A dislocation cell structure like that observed in the heavily deformed ferrite grain is seen. This structure is also characterized by high internal stresses, as indicated by bent extinction contours inside grains. The average size of the dislocation cell is around 100 nm. The existence of cementite particles is confirmed both by the morphology and the selected-area diffraction patterns (SADPs).

Figure 3 shows the TEM images of the area near the surface of a particle milled for 360 ks. Two types of microstructures were observed. One is a layered nanocrystalline ferrite structure with a thickness of 10 to 50 nm, as shown in Figure 3(a). The bright-field image and SADP of this region show that cementite still remains as fine particles, although the amount of it becomes less. It is deduced that cementite particles receive severe deformation, fracture into small particles, and gradually dissolve into nanocrystalline ferrite grains with the evolution of the ball-milling process. The HREM image (Figure 3(b)) of the layered nanocrystalline ferrite indicates that the grain boundary having a layered nanostructure, is not of the dislocation cell-wall type, but of a granular type, like a conventional high-angle grain boundary. The misorientation angle between the adjacent layer was determined to be high. The misorientation angles in Figure 3(b), measured from the (110) plane in each layer, were 30 deg. There exists microstress within the nanocrystalline ferrite layers, which is attributed to the existence of dislocations within layers. The other type of microstructure

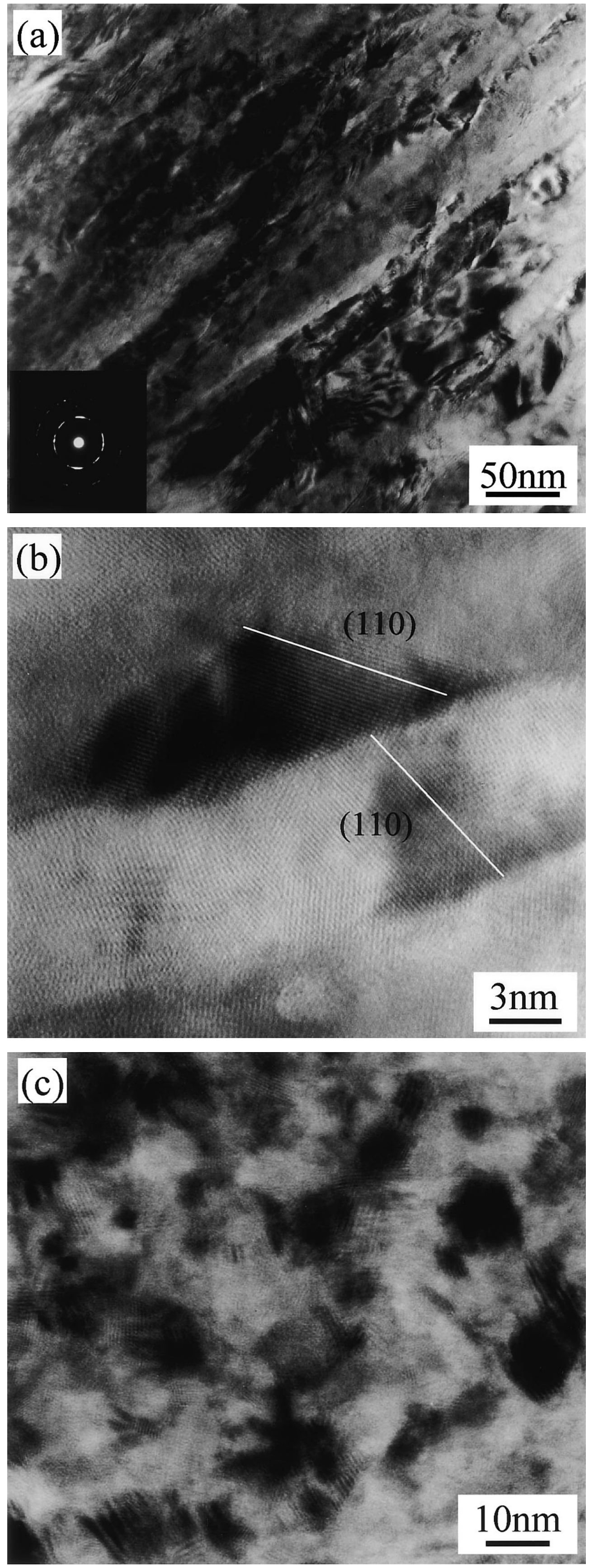

Fig. 3—Typical TEM images of the nanocrystalline ferrite in the powder milled for 360 ks: (*a*) layered nanocrystalline ferrite, (*b*) high-resolution image of layered nanocrystalline ferrite, and (*c*) equiaxed nanocrystalline ferrite.

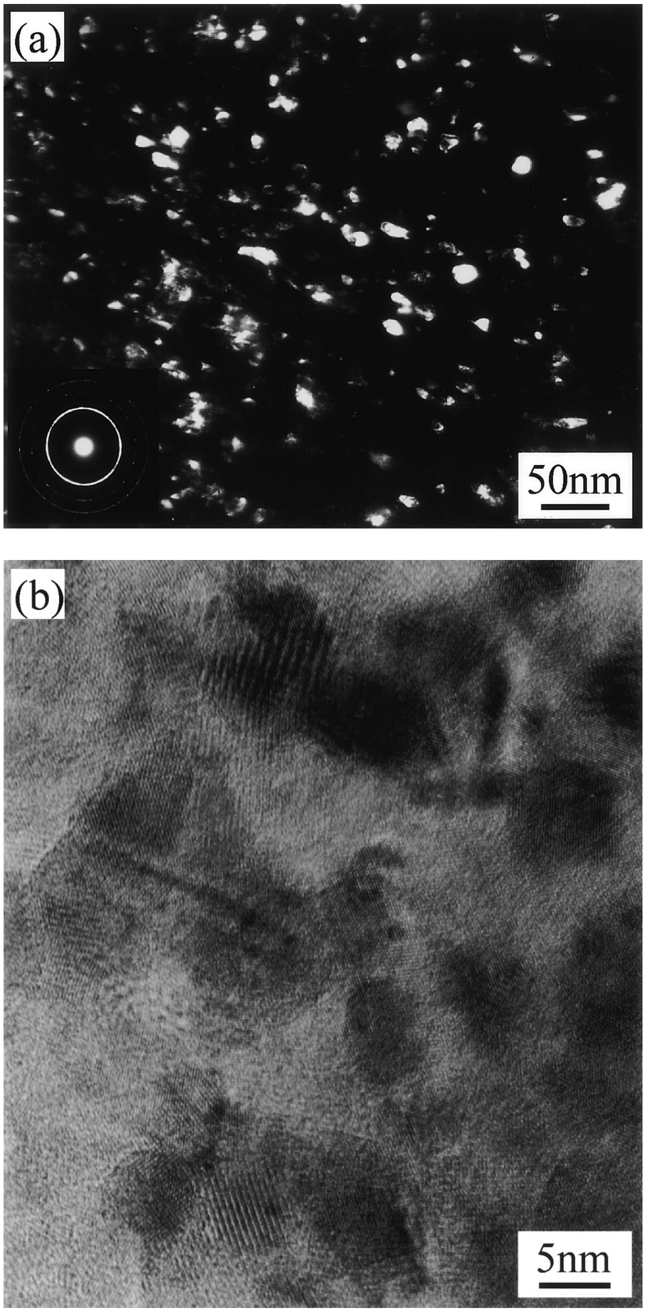

Fig. 4—Typical TEM images of the uniformly distributed equiaxed nanocrystalline ferrite in the powders milled for 1800 ks: (*a*) lower magnification and (*b*) high-resolution image.

is equiaxed nanocrystalline ferrite of 10 nm in average diameter (Figure 3(c)). This indicates that layered nanocrystalline ferrite will evolve into equiaxed nanocrystalline ferrite with further deformation.

Figure 4 shows the TEM images of the Fe-0.89C spheroidite powders milled for 1800 ks. The microstructure of the powders consists of uniform, equiaxed nanocrystalline ferrite grains ranging from 5 to 10 nm in size (Figure 4(a)). The HREM image (Figure 4(b)) shows a random orientation of grains with a large misorientation. No dislocations exist within the equiaxed nanocrystalline ferrite (Figure 4(b)). The SADP indicates that the cementite particles have dissolved completely.

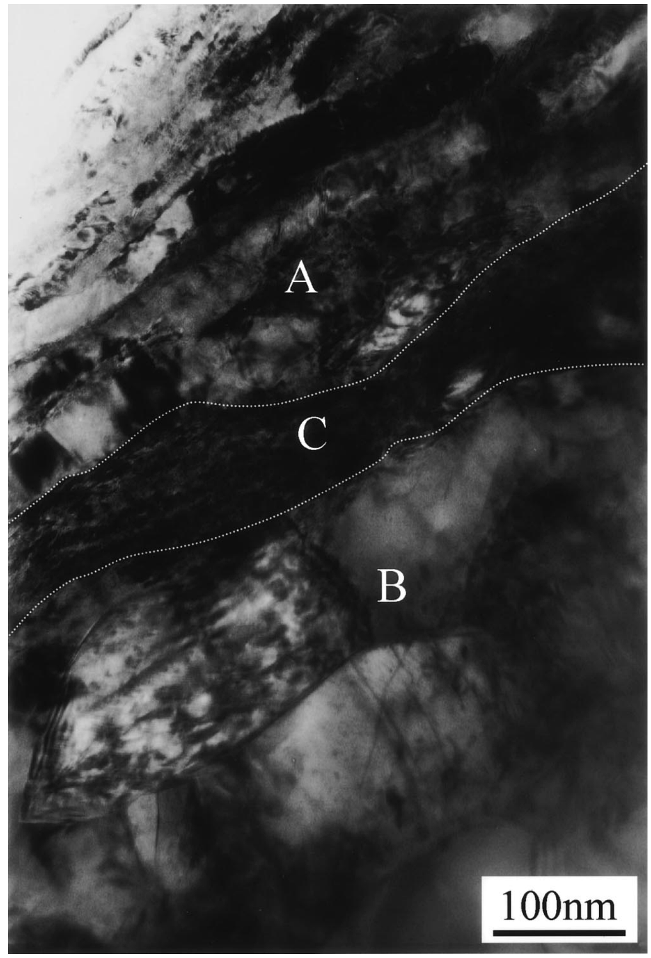

Fig. 5—TEM image showing the boundary between the work-hardened ferrite and layered nanocrystalline ferrite in the powder milled for 360 ks. "A" indicates the layered nanocrystalline ferrite region, "B" the interior work-hardened ferrite region, and "C" the boundary.

The most interesting result was the finding of the boundary between the deformed work-hardened grains and the layered nanocrystalline grains, as shown in Figure 5. In the upper part (A) of the figure, the layered nanocrystalline ferrite, with an average thickness of 10 to 50 nm, is shown. The lower part (B) of the figure shows some deformed grains larger than 100 nm, where the dislocations in the grains and some subgrain boundaries are clearly visible. Between them, there exists a narrow band region (C) about 50 to 100 nm thick, where a high density of dislocations is believed to exist. It should be noted that the structure change occurs in a very narrow region. This indicates that there exists a sharp critical deformation condition that separates the work-hardened and layered nanocrystalline structure.

3. *Microhardness evolution results*

Figure 6 shows the dynamic microhardness across the boundary between the nanocrystalline ferrite and work-hardened ferrite. The two types of microstructures show quite different microhardnesses, that is, about 4 GPa in the work-hardened region and about 10 GPa in the nanocrystalline region. A drastic change in hardness was observed at the boundary where the microstructure changes. The microhardness evolution with ball-milling time is shown in Figure 7. The microhardness of the interior work-hardened ferrite

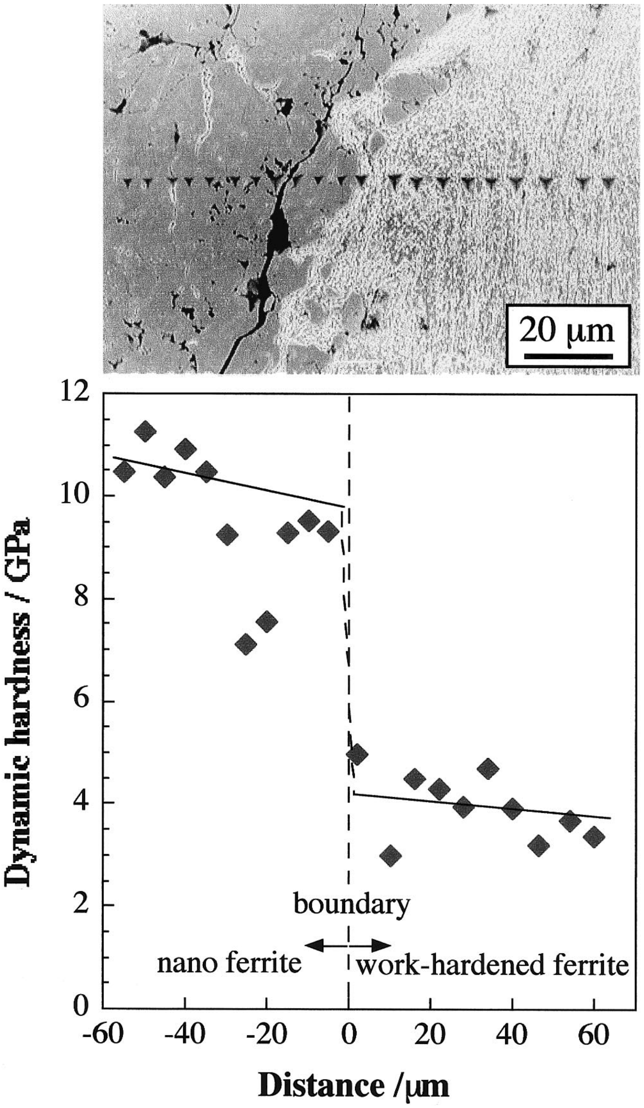

Fig. 6—Microstructure and dynamic microhardness profile across the boundary of the nanocrystalline ferrite and work-hardened ferrite regions in the 360 ks ball-milled sample.

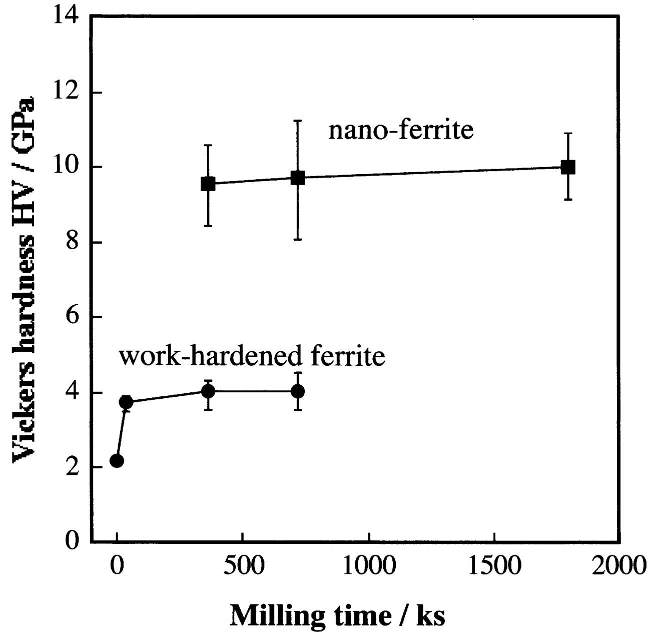

Fig. 7—Microhardness evolution of the two types of microstructures with increasing milling time.

region increases from 2.2 to 3.7 GPa after 36 ks milling. The further milling to 720 ks does not change the microhardness, and the work-hardened region no longer remains after 1800 ks of milling. In contrast, the microhardness of the nanocrystalline ferrite region is as high as 9.5 GPa after milling for 360 ks, when it first appears. Further milling up to 1800 ks does not change the microhardness of the nanocrystalline ferrite region. It should be noted that there is a substantial difference in microhardness between the two microstructures. The distinctive difference in microhardness indicates that the strengthening mechanisms of the two types of microstructures are different.

B. *Microstructural and Microhardness Evolution by Annealing*

1. *Microstructural evolution by annealing*

Figure 8 shows the annealed microstructures around the boundary between the work-hardened (right-hand side in each picture) and nanocrystalline ferrite regions (left-hand side in each picture) of the powders milled for 360 ks. After annealing at 673 K for 3.6 ks (Figure 8(a)), conventional discontinuous recrystallization takes place in the work-hardened ferrite region, leading to the formation of recrystallized ferrite grains with an average grain size of about 0.5 μm. In the nanocrystalline ferrite region, the reprecipitation of fine cementite can be observed, but no significant change is seen in the ferrite grain. The TEM observation shows that the grain size of nanocrystalline ferrite after annealing at 673 K is only about 40 nm, showing a slow grain growth rate. It was found the grain boundaries of annealed nanocrystalline ferrite are irregular and curved, indicating that the grain growth does not stem from conventional discontinuous recrystallization (Figure 9). The grain-boundary morphology of annealed nanocrystalline ferrite is clearer than that of as-milled nanocrystalline ferrite, where the latter shows an ambiguous morphology due to high distortions and high internal stresses near the grain boundary.

When annealing at 873 K for 3.6 ks (Figure 8(b)), the obvious grain growth of recrystallized ferrite can be observed in the work-hardened ferrite region. In the nanocrystalline ferrite region, the progress of reprecipitation of cementite particles and the grain growth of nanocrystalline ferrite can be seen by SEM observations. The average grain size of nanocrystalline ferrite (about 0.2 μm) is much smaller than that of recrystallized ferrite (about 1.5 μm).

When annealing at 1073 K for 3.6 ks (Figure 8(c)), austenitization occurs both in the work-hardened ferrite and nanocrystalline ferrite regions; hence, a pearlite structure forms in these regions during the subsequent cooling. The interface between the original nanocrystalline ferrite and work-hardened ferrite regions becomes blurred.

2. *Microhardness evolution by annealing*

Figure 10 shows the microhardness evolution of the work-hardened and nanocrystalline ferrite regions as a function of isochronal annealing temperature. In both regions, the

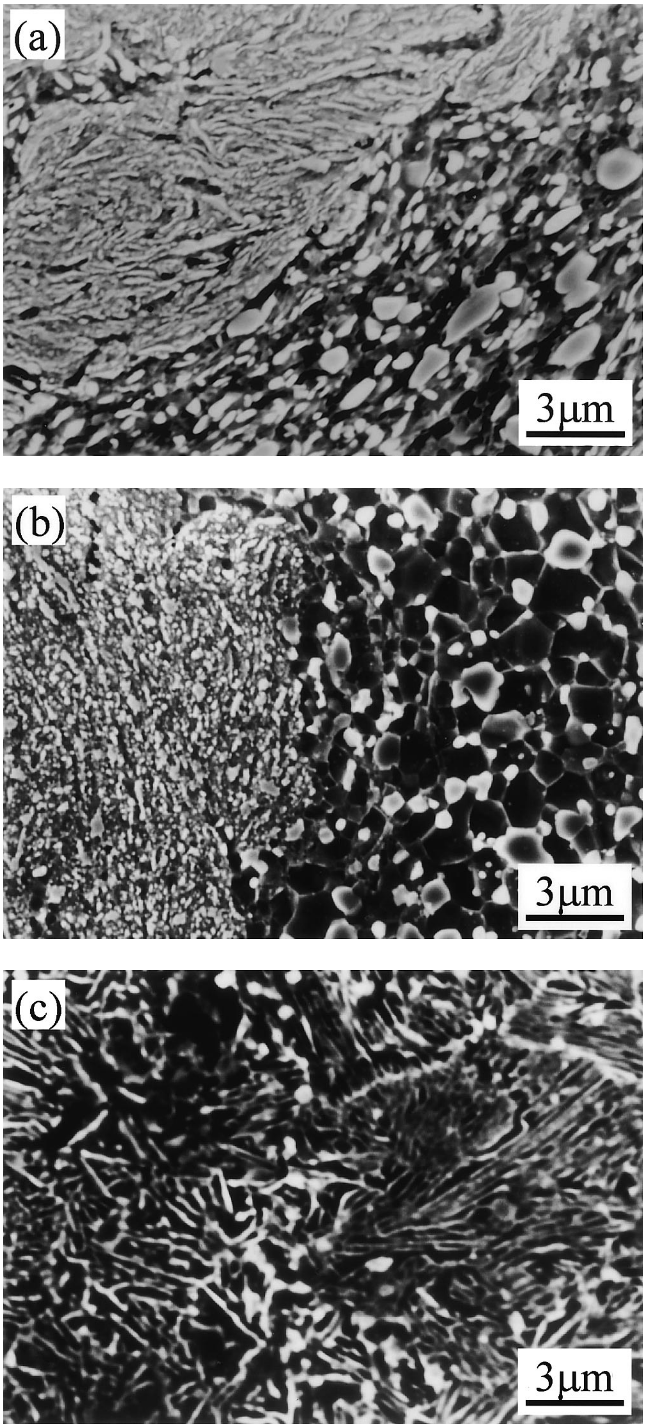

Fig. 8—Microstructure evolution of the two types of microstructures in the 360 ks ball-milled powders after annealing at (*a*) 673 K, (*b*) 873 K, and (*c*) 1073 K for 3.6 ks.

Fig. 9—HREM image of the nanocrystalline ferrite in the 360 ks ball-milled powders after annealing at 673 K for 3.6 ks.

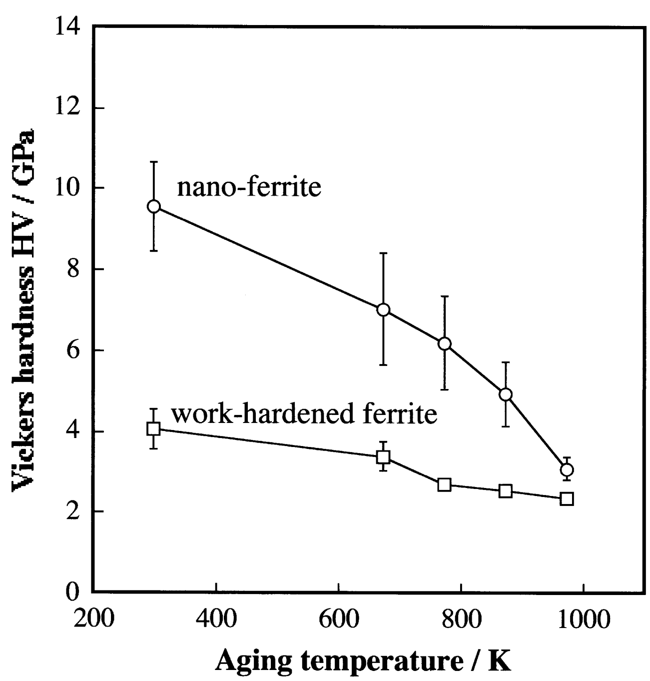

Fig. 10—Microhardness evolution of the two types of microstructures in the 360 ks ball-milled powders with annealing at different temperatures for 3.6 ks.

microhardness decreases with increasing annealing temperature. The microhardness decrease in the work-hardened ferrite region is attributed to the recrystallization and grain growth. However, the microhardness decrease in the nanocrystalline ferrite is attributed to the grain growth of nanocrystalline ferrite and reprecipitation of cementite. As mentioned previously, since the grains in the nanocrystalline ferrite grow continuously, a gradual decrease of microhardness is obtained.

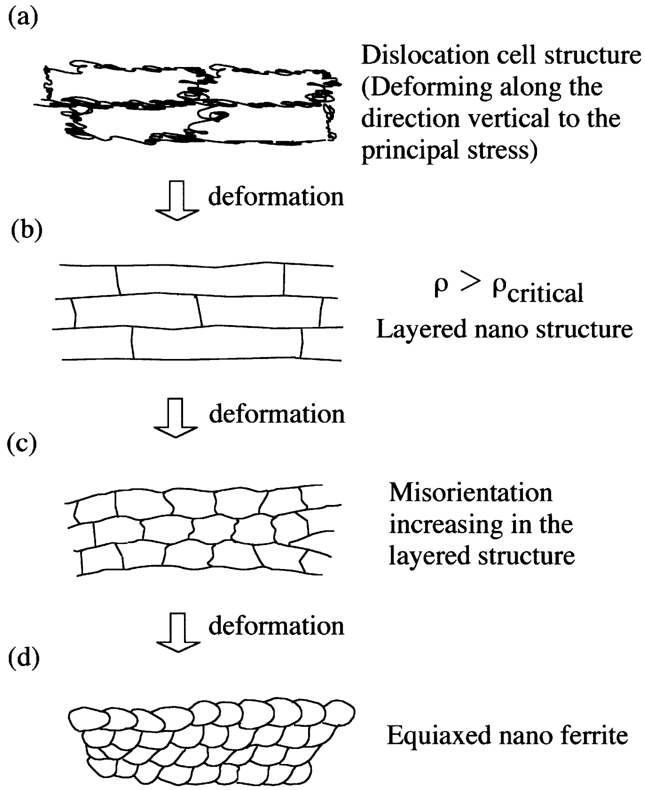

Fig. 11—(*a*) through (*d*) A schematic drawing of nanocrystalline ferrite formation by ball milling.

IV. DISCUSSIONS

A. *Nanocrystalline Ferrite Formation during Ball Milling*

It has been accepted that heavy deformation is a necessary condition for nanostructure formation by ball milling. There are many parameters in deformation, such as stress modes (shear, compressive, tensile, *etc.*), degree of strain, strain rate, temperature, *etc.* The dominant factor that controls the formation of nanostructure is still unclear. In practical deformation, it is very difficult to separate the individual effect of these factors because they interact with each other. Fecht[33] proposed that high-shear deformation is a necessary condition for nanostructure formation. He also found that friction could induce nanostructure formation on a wear surface.[34] Recent research showed that heavy plastic deformation at the wheel-rail contact zone causes nanostructure formation on the surface layer of railway tracks.[35] The aforementioned results indicate that various kinds of deformation modes can induce the nanostructure. Ball milling is a complicated deformation process which includes many strain modes, and this may enhance the formation of nanostructure.

The present SEM and TEM observations revealed a microstructural evolution for nanocrystallization in ball milling, and it is shown schematically in Figure 11. At the early stage of ball milling, the dislocation density increases and cell structure is developed in ferrite grains with milling time (Figure 11(a)). With further deformation, the misorientation between the adjacent cells increases and the size of dislocation cells decreases. It has been proposed that when the dislocation density in the cell walls reaches a critical value, a transition from a cellular to granular structure will take place to reduce the energy of the system (Figure 11(b)).[10,11,21,23] This transition is suggested to involve a dynamic recovery and dynamic continuous recrystallization, which is assisted by the temperature rise due to ball collisions. Since the ball collisions take place in a very short time at only a quite limited surface area of the powders, the strain rate is sufficiently high. A high strain rate (determining the dislocation generation rate) not only leads to the high dislocation density, but also causes the temperature to rise. When two dislocations with opposite sign meet on the same slip plane, they annihilate each other and the dislocation energy (mostly elastic energy) dissipates into heat. Since the dislocation density in a cell wall is much higher than that in the interior of cells, dislocation annihilation occurs mostly at cell walls. When the strain rate is high, the heat accumulation at the cell walls would be sufficiently high. Hence, the temperature rise at the cell walls becomes high enough to induce not only dynamic recovery but also dynamic continuous recrystallization. Consequently, layered nanocrystalline ferrite with a granular structure forms. In the study on synthesizing nanocrystalline Zn by cryomilling methods, dynamic recrystallization was also considered to happen at a low milling temperature (ball milling at liquid nitrogen temperature) from the energy change point of view. This dynamic recrystallization event leads to the formation of nanocrystalline grains with orientations different from the original grain orientation.[17]

When the layered nanocrystalline ferrite forms, further deformation will lead to the fragmentation of the layers (Figure 11(c)). The layered structure is refined to a much thinner thickness of about 10 nm and further transforms to an equiaxed nanocrystalline grain of 5 to 10 nm in size. Once an equiaxed nanocrystalline structure is achieved, further refinement will not occur, since deformation takes place mainly by grain-boundary sliding.[36] A random distribution of orientations of equiaxed nanocrystalline grains with large misorientations will be achieved by this grain-boundary sliding (Figure 11(d)).

B. *Cementite Dissolution during Nanocrystalline Ferrite Formation*

In the layered nanocrystalline structure, spherical cementite particles are hard to observed by SEM (Figure 1(b)). The TEM observations (Figure 3(a)) showed that only a small volume fraction of fine cementite particles remains in the layered nanocrystalline ferrite region, and cementite particles are completely dissolved when the layered nanostructure changes into an equiaxed nanostructure upon further deformation (Figure 4). As a hard second phase, cementite might assist the formation of nanocrystalline ferrite by increasing the dislocation density during ball milling. When nanocrystalline ferrite forms, the hardness of the nanocrystalline ferrite reaches the same level of cementite (about 10 GPa[37]). Cementite particles are easy to deform or fracture to finer particles when the matrix ferrite becomes nanocrystalline. Such fragmented cementite particles can dissolve into ferrite, as analyzed by Korznikov *et al.*[29]

A large number of arguments have been made on the dissolution mechanism of cementite into a ferrite matrix. Cementite was present as fragmented nanoscale particles, and partial dissolution of cementite was generally observed in heavily drawn pearlite wire.[27,28] It was observed[29] by a three-dimensional (3-D) atom probe that the carbon content in cementite decreased from 25 at. pct to about 10 at. pct and that the carbon content in ferrite increased at the same time. When the extremely heavy deformation was applied, cementite completely dissolved into ferrite. It can be assumed that the fragmented cementite particle become smaller than the critical nucleus for cementite precipitation in a supersaturated solid solution of carbon in ferrite. When this condition is achieved, all the cementite particles will dissolve into ferrite. There are three possible positions for carbon atoms from cementite to locate in ferrite, *i.e.*, near an edge dislocation, ferrite grain boundary, or at a conventional interstitial site of bcc ferrite. Since a high density of dislocations was not observed in nanostructured ferrite, the dislocation site can be excluded. The ferrite grain boundary seems a good candidate for a carbon atom to locate to, since more space is available than inside a grain. Hidaka *et al.*[25,26] considered that carbon from cementite exists as the amorphous layer around the nanocrystalline ferrite grain boundaries. However, 3-D atom-probe analysis showed a uniform distribution of carbon atoms[29] rather than the nonuniform distribution which could be expected if carbon had segregated to the grain boundary. Thus, the only possible site for a carbon atom in ferrite is the regular interstitial site. But, differential scanning calorimetry (DSC) analysis indicates that there is a difference between the precipitation behaviors of cementite from martensite and from nanocrystalline ferrite.[39] It seems that in nanostructured ferrite, cementite precipitates directly from a supersaturated solid solution, while in martensite, a ε-carbide forms prior to cementite formation. This might be the reason of the observed difference in DSC results. This subject should be considered in more detail in a future study.

C. *Thermal Stability of Nanocrystalline Ferrite*

Our results show that the annealing behavior of nanocrystalline ferrite is intrinsically different from that of work-hardened ferrite. Conventional discontinuous recrystallization takes place in the work-hardened ferrite region due to the existence of a high density of dislocations. In contrast, continuous grain growth occurs in the nanocrystalline ferrite region instead of conventional recrystallization, because of the presence of dislocation-free small grains with a large misorientation. Similar results were obtained in the study on annealed samples of mechanically milled iron powders.[20,21]

Grain growth occurs in polycrystalline materials to decrease the grain-boundary energy and, hence, the total energy of the system. Since nanocrystalline materials have a highly disordered, large grain-boundary component (and, therefore, they are in a high-energy state), the driving force for grain growth is high. Hence, a high grain growth rate in nanocrystalline materials was expected. However, contrary to the expectation, a low grain growth rate was observed in various nanocrystalline materials. The inherent stability of the nanocrystalline grains has been explained on the basis of structural factors such as narrow grain-size distribution, equiaxed grain morphology, low-energy grain-boundary structures, relatively flat grain-boundary configurations, and the porosity present in some samples.[2] Additionally, grain-boundary Zener drag and triple-junction drag have been found to be significant in retarding grain growth.[40]

Zener drag (where a particle interacts with grain boundary to reduce the energy of the boundary-particle system and restrain the grain-boundary movement) and solute drag can slow down the grain-growth kinetics by reducing the driving force or the grain-boundary mobility. The ball-milled materials could be contaminated by some impurities either from the milling materials or milling atmosphere. Besides the impurities, the carbon dissolved in the nanocrystalline ferrite is assumed to contribute to this effect. With the increase of annealing temperature, cementite particles begin to reprecipitate along the grain boundaries. The fine cementite particles can also play the role of pinning the movement of grain boundaries. Hence, at a lower annealing temperature, the grain growth rate of nanocrystalline ferrite is much lower than that of work-hardened ferrite. However, at a higher annealing temperature (more than 873 K), the cementite particles become so large due to the Ostward coalescence that they lose the effect on retarding the movement of grain boundaries of nanocrystalline ferrite; consequently, the grain growth of ferrite becomes obvious. Thus, the low grain growth rate of nanocrystalline ferrite in the ball-milled spheroidite specimen is enhanced by carbon.

V. CONCLUSIONS

The SEM and TEM observations on the ball-milled Fe-0.89C spheroidite alloy show that the ferrite nanocrystallization process by heavy deformation in ball milling is realized through the following steps: (1) the density of dislocations increases and dislocation cells form due to deformation; (2) localized deformation leads to a high strain and strain rate, which cause the transition from the dislocation cells into a granular structure by dynamic recovery and recrystallization, and hence, layered nanocrystalline ferrite with a thickness less than 50 nm forms; and (3) further deformation increases the misorientation of grain boundaries, and then the equiaxed nanocrystalline ferrite grains of 5 to 10 nm in size form. Cementite dissolves during the process of nanocrystalline ferrite formation. The nanocrystalline ferrite shows much higher microhardness than the work-hardened ferrite. The annealing behaviors of nanocrystalline ferrite and work-hardened ferrite are intrinsically different. Conventional discontinuous recrystallization takes place in the work-hardened ferrite region, while continuous grain growth occurs in the nanocrystalline ferrite region during annealing. The microhardness of the annealed nanocrystalline ferrite is still higher than that of annealed work-hardened ferrite under the same annealing condition.

ACKNOWLEDGMENTS

This work is partly supported by the Ferrous Super Metal Consortium of Japan under the auspices of NEDO and by the Strategic Research Project of Iron and Steel Institute of Japan. One of the authors (Y. Xu) thanks AIEJ for supplying the Japanese Government (Monbusho) Scholarship to carry out this work in Japan.

REFERENCES

1. H. Gleiter: *Acta Mater.*, 2000, vol. 48, pp. 1-29.
2. C. Suryanarayana: *Int. Mater. Rev.*, 1995, vol. 40, pp. 41-64.

3. J.S.C. Jang and C.C. Koch: *Scripta Mater.*, 1990, vol. 24, pp. 1599-1604.
4. E. Hellstern, H.J. Fecht, C. Garland, and W.L. Johnson: *Mater. Res. Soc. Symp. Proc.*, 1989, vol. 132, pp. 137-42.
5. H.J. Fecht, E. Hellstern, Z. Fu, and W.L. Johnson: *Metall. Trans. A*, 1990, vol. 21A, pp. 2333-37.
6. K. Lu, W.D. Wei, and J.T. Wang: *Scripta Metall. Mater.*, 1990, vol. 24, pp. 2319-23.
7. C. Suryanarayana and F.H. Froes: *Nanostruct. Mater.*, 1993, vol. 3, pp. 147-53.
8. R.Z. Valiev, A.V. Korznikov, and R.R. Mulyukov: *Phys. Met. Metall.*, 1992, vol. 73, pp. 373-83.
9. D.H. Shin, B.C. Kim, Y.-S. Kim, and K.-T. Park: *Acta Mater.*, 2000, vol. 48, pp. 2247-55.
10. R.Z. Valiev, R.K. Islamgaliev, and I.V. Alexandrov: *Progs. Mater. Sci.*, 2000, vol. 45, pp. 103-89.
11. R.Z. Valiev, YU. V. Ivanisenko, E.F. Rauch, and B. Baudelet: *Acta Mater.*, 1996, vol. 44, pp. 4705-12.
12. C.C. Koch: *Nanostruct. Mater.*, 1993, vol. 2, pp. 109-29.
13. C.C. Koch: *Nanostruct. Mater.*, 1997, vol. 9, pp. 13-22.
14. H.J. Fecht: *Nanostruct. Mater.*, 1995, vol. 6, pp. 33-41.
15. H.J. Fecht, E. Hellstern, Z. Fu, and W.L. Johnson: *Adv. Powder Metall.*, 1989, vol. 1, pp. 111-22.
16. J.Y. Huang, Y.K. Wu, and H.Q. Ye: *Acta Mater.*, 1996, vol. 44, pp. 1201-09.
17. X. Zhang, H. Wang, J. Narayan, and C.C. Koch: *Acta Mater.*, 2001, vol. 49, pp. 1319-26.
18. H.H. Tian and M. Atsmon: *Acta Mater.*, 2001, vol. 49, pp. 1255-61.
19. Y.H. Zhao, H.W. Sheng, and K. Lu: *Acta Mater.*, 2001, vol. 49, pp. 365-75.
20. S. Takaki and Y. Kimura: *J. Jpn. Soc. Powder Powder Metall.*, 1999, vol. 46, pp. 1235-40.
21. J. Yin, M. Umemoto, Z.G. Liu, and K. Tsuchiya: *Iron Steel Inst. Jpn. Int.*, 2001, vol. 41, pp. 1389-96.
22. Z.G. Liu, X.J. Hao, K. Masuyama, K. Tsuchiya, M. Umemoto, and S.M. Hao: *Scripta Mater.*, 2001, vol. 44, pp. 1775-79.
23. M. Umemoto, Z.G. Liu, X.J. Hao, K. Masuyama, and K. Tsuchiya: *Mater. Sci. Forum*, 2001, vols. 360–362, pp. 167-74.
24. M. Umemoto, Z.G. Liu, Y. Xu, and K. Tsuchiya: *Mater. Sci. Forum*, vols. 386–388, pp. 323-28.
25. H. Hidaka, Y. Kimura, and S. Takaki: *J. Jpn. Soc. Powder Powder Metall.*, 1999, vol. 46, pp. 1256-60.
26. H. Hidaka, Y. Kimura, and S. Takaki: *Tetsu-to-Hagané*, 1999, vol. 85, pp. 52-58.
27. H.G. Read, W.T. Reynolds Jr, K. Hono, and T. Tarui: *Scripta Mater.*, 1997, vol. 37, pp. 1221-30.
28. M.H. Hong, W.T. Reynolds Jr, T. Tarui, and K. Hono: *Metall. Mater. Trans. A*, 1999, vol. 30A, pp. 717-27.
29. K. Hono, M. Ohnuma, M. Murayama, S. Nishida, A. Yoshie, and T. Takahashi: *Scripta Mater.*, 2001, vol. 44, pp. 977-83.
30. C.H. Moelle and H.J. Fecht: *Nanostruct. Mater.*, 1995, vol. 6, pp. 421-24.
31. T.R. Marlow and C.C. Koch: *Acta Mater.*, 1997, vol. 45, pp. 2177-86.
32. K.W. Liu and F. Mucklick: *Acta Mater.*, 2001, vol. 49, pp. 395-403.
33. H.J. Fecht: in *Nanomaterials: Synthesis, Properties and Applications*, A.S. Edelstain and R.C. Cammarata, eds., Institute of Physics Publications, Bristol, 1996, p. 127.
34. H.J. Fecht: *Scripta Mater.*, 2001, vol. 44, pp. 1719-23.
35. W. Lojkowski, M. Djahanbakhsh, G. Burkle, S. Gierlotka, S. Gielotka, W. Zielinski, and H.J. Fecht: *Mater. Sci. Eng.*, 2001, vol. A303, pp. 197-208.
36. J. Karch, R. Birringer, and H. Gleiter: *Nature*, 1987, vol. 330, pp. 556-58.
37. M. Umemoto, Z.G. Liu, H. Takaoka, M. Sawakami, K. Tsuchiya, and K. Masayama: *Metall. Mater. Trans. A*, 2001, vol. 32A, pp. 2127-31.
38. A.V. Korznikov, Yu. V. Ivanisenko, D.V. Laptionok, I.M. Safarov, V.P. Pilyugin, and R.V. Valiev: *Nanostruct. Mater.*, 1994, vol. 4, pp. 159-67.
39. X.J. Hao, Z.G. Liu, K. Masuyama, T. Rikimaru, M. Umemoto, K. Tsuchiya, and S.M. Hao: *Mater. Sci. Tech.*, 2001, vol. 17, pp. 1347-52.
40. K. Lu: *Nanostruct Mater.*, 1993, vol. 2, pp. 643-52.